



Unveiling the impact of flooding and salinity on iron oxides-mediated binding of organic carbon in the rhizosphere of *Scirpus mariqueter*

Yuxin Bi^{a,b}, Xiaoqing Gao^{a,b}, Lin Su^{a,b}, Ying Lei^{a,b}, Tianyou Li^{a,b}, Xinhan Dong^{a,b}, Xiuzhen Li^{a,b}, Zhongzheng Yan^{a,b,*}

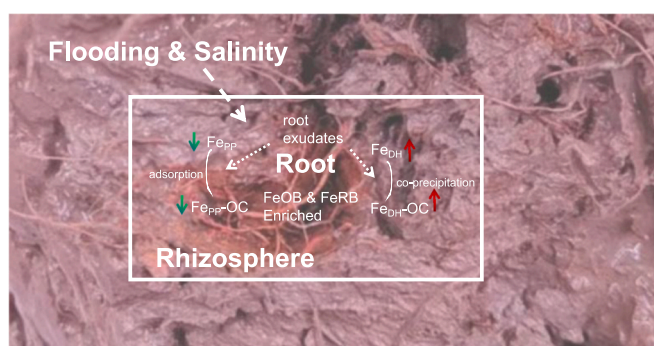
^a State Key Laboratory of Estuarine and Coastal Research, Institute of Eco-Chongming, East China Normal University, Shanghai, China

^b Yangtze Delta Estuarine Wetland Ecosystem Observation and Research Station, Ministry of Education & Shanghai Science and Technology Committee, China

HIGHLIGHTS

- Elevated flooding and salinity lead to a greater portion of amorphous Fe (hydro) oxides.
- Increased flooding and salinity lowered rhizosphere sediment Fe_{pp} content.
- Elevated salinity raised the Fe_{pp}-OC content, whereas prolonged flooding lowered it.
- Increased flooding and salinity enhanced the crystalline Fe-OC content in the sediment.
- The sediment Fe-OC remains stable amidst short-term changes in flooding and salinity.

GRAPHICAL ABSTRACT



ARTICLE INFO

Editor: Jan Vymazal

Keywords:

Salinity
Inundation
Soil organic carbon
Iron-bound organic carbon
Scirpus mariqueter
Rhizosphere

ABSTRACT

The abundant Fe (hydr-) oxides present in wetland sediments can form stable iron (Fe)-organic carbon (OC) complexes (Fe-OC), which are key mechanisms contributing to the stability of sedimentary OC stocks in coastal wetland ecosystems. However, the effects of increased flooding and salinity stress, resulting from global change, on the Fe-OC complexes in sediments remain unclear. In this study, we conducted controlled experiments in a climate chamber to quantify the impacts of flooding and salinity on the different forms of Fe (hydr-) oxides binding to OC in the rhizosphere sediments of *S. mariqueter* as well as the influence on Fe redox cycling bacteria in the rhizosphere. The results of this study demonstrated that prolonged flooding and high salinity treatments significantly reduced the content of organo-metal complexes (Fe_{pp}) in the rhizosphere. Under high salinity conditions, the content of Fe_{pp}-OC increased significantly, while flooding led to a decrease in Fe_{pp}-OC content, inhibiting co-precipitation processes. The association of amorphous Fe (hydr-) oxides (Fe_{HH}) with OC showed no significant differences under different flooding and salinity treatments. Prolonged flooding significantly increased the relative abundance of Fe-reducing bacteria (FeRB) *Deferrisoma* and *Geothermobacter* and decreased polyphenol oxidase in the rhizosphere, while the relative abundance of Fe-oxidizing bacteria (FeOB) *Paracoccus* and *Pseudomonas* decreased with increasing salinity and duration of flooding. Overall, short-term water and salinity stress promoted the binding of Fe_{DH} to OC in the rhizosphere of *S. mariqueter*, leading to a reduction in the OC content held by Fe_{pp}. However, there were no significant differences observed in the OC stocks or the total

* Corresponding author at: State Key Laboratory of Estuarine and Coastal Research, East China Normal University, 500 Dongchuan Road, Shanghai, China.

E-mail address: zzyan@sklec.ecnu.edu.cn (Z. Yan).

<https://doi.org/10.1016/j.scitotenv.2023.168447>

Received 20 August 2023; Received in revised form 19 October 2023; Accepted 7 November 2023

Available online 11 November 2023

0048-9697/© 2023 Elsevier B.V. All rights reserved.

Fe-OC content in the rhizosphere sediments. The findings suggest a degree of consistency in the Fe-OC of the “plant-soil” complex system within tidal flat wetlands, showing resilience to abrupt shifts in flooding and salinity over short periods.

1. Introduction

Salt marshes are important coastal wetland ecosystems known for their ability to sequester carbon due to anaerobic sedimentary conditions (Tang et al., 2011; Hopkinson et al., 2012; Lovelock and Duarte, 2019). The sediments of coastal wetland are rich in iron (Fe) and its oxides (Weaver and Tarney, 1984), particularly Fe (hydr-) oxides, which are closely associated with sediment organic carbon (OC) in wetland ecosystems (Yu et al., 2021). Fe (hydr-) oxides have a significant surface area that promotes the formation of stable organic complexes (Fe-OC) through adsorption, co-precipitation, and complexation processes. These complexes of Fe-OC safeguard sediment OC against microbial breakdown, thereby increasing its resilience (Wiseman and Püttmann, 2006; Kleber et al., 2007; Kögel-Knabner et al., 2008; Coward et al., 2018; Sowers et al., 2019). The binding stability of sediment OC depends on the crystallinity of Fe (hydr-) oxides, with crystalline forms exhibiting greater stability against microbial activity (Yu et al., 2021). The redox conditions induced by tidal fluctuations and microbial activity cause transformations in the valence state of Fe in sediments and the morphology of Fe (hydr-) oxides. Prolonged inundation leads to decreased sediment redox potential, favoring the formation of amorphous Fe (hydr-) oxides with low nucleation interface energy (Li et al., 2020a). The alternating aerobic and anaerobic conditions in tidal wetlands contribute to the dissolution and precipitation of Fe (hydr-) oxides, thereby affecting their maturation process (Thompson et al., 2006). Nevertheless, the complete impact and mechanisms of these Fe (hydr-) oxide transformations on the preservation and stability of sediment OC under changing redox conditions remain largely unexplored.

The morphological transformations of Fe (hydr-) oxides become increasingly intricate in the rhizosphere of plants, primarily due to the influence of wetland plant root exudations. Plant roots fix atmospheric CO₂ through photosynthesis and release organic matter into the rhizosphere soil through root exudation, including sugars, proteins, amino acids, low molecular weight organic acids (LMWOAs), etc. These root exudates (REs) serve as significant sources of organic matter in the rhizosphere. The type and quantity of REs influence the microbial community structure and activity by affecting soil C sequestration (Bertin et al., 2003; Yuan et al., 2015; Canarini et al., 2018). LMWOAs exuded by roots can promote the formation of weakly crystalline Fe (hydr-) oxides (Yu, 2018). Moreover, plant roots and associated microbial communities play crucial roles in the formation, transformation, and turnover of Fe (hydr-) oxides and related OC in the rhizosphere and adjacent soil. The rhizosphere, characterized by high OC concentrations and microaerobic conditions, promotes the proliferation of Fe redox cycling bacteria, such as Fe-oxidizing bacteria (FeOB) and Fe-reducing bacteria (FeRB) (Kaplan et al., 2016). Radial oxygen loss (ROL) from roots creates redox potential and Fe (hydr-) oxide concentration gradients between the root surface and the rhizosphere. Under these microaerobic conditions, Fe (II) remains relatively stable, and FeOB becomes the primary driving force for weakly crystalline Fe (hydr-) oxide formation (Chen et al., 2018). Dissimilatory Fe (III) reduction by Fe (III)-reducing microorganisms is an important mechanism for organic matter oxidation. The rate of dissimilatory Fe (III) reduction in coastal wetlands depends on the availability of OC (electron donors) or amorphous Fe (hydr-) oxides (electron acceptors) (Yu et al., 2021).

Climate change-induced sea level rise has increased the frequency of extreme tidal events and storms in coastal wetlands, leading to saltwater intrusion and reduced productivity and C sequestration capacity of tidal marsh plants (Kirwan and Megonigal, 2013; Kirwan et al., 2016). Flooding and salinity are two critical environmental factors in tidal

wetlands that significantly impact the growth and metabolism of salt marsh plants, as well as the storage of C in sediment. Increasing salinity reduces soil microbial diversity (Yuan et al., 2007; Tong et al., 2019). This also results in decreased plant biomass and productivity, leading to reduced C inputs from plants and influencing sediment OC reserves. Longer flood durations influence the transformation of valence states of Fe and the morphology of sedimentary Fe (hydr-) oxides. Flooding can increase the extractable Fe content in sediments and alter the occurrence of forms of Fe (hydr-) oxides by changing soil pH (Saleh et al., 2013; Gartzia-Bengoetxea et al., 2020; Lyu et al., 2021). Prolonged flooding can lead to a decrease in sediment OC stocks (Huang et al., 2022). However, flooding can also enhance plant root exudation, promoting the release of more OC by plant roots, altering the sediment's physicochemical environment, reducing the OC mineralization rate, and facilitating its preservation (Henry et al., 2007; Chapman et al., 2019).

Currently, the comprehensive impact of flooding, salinity, and interactions among salt marsh plants on the phase transformation of Fe (hydr-) oxides in the rhizosphere and the stability of Fe-OC binding remain unclear. Therefore, we focused on the pioneer species *Scirpus marquetei* in the Yangtze Estuary and conducted controlled experiments in a climate chamber to study how variations in flooding and salinity conditions affect the morphological changes of Fe (hydr-) oxides in the plant's rhizosphere sediments and their interaction with sediment OC. Additionally, we monitored the changes in bacterial composition in the rhizosphere sediments under different flooding and salinity conditions using high-throughput sequencing of 16s rDNA, and tracked the relative abundance shifts of Fe redox cycling bacteria. This analysis aimed to investigate the relationship between these indicators and the morphological changes of Fe (hydr-) oxides as well as their binding with OC.

2. Materials and methods

2.1. Experimental setup

We gathered the seeds and sediments of *S. marquetei* from Chongming Dongtan Wetland (31°25'–31°38'N, 121°50'–122°05'E) to conduct our experiments. Table S1 presents the physicochemical properties of the sediments. The mature seeds of *S. marquetei* were mixed with fine sea sand at a volume ratio of 1:2 and stored in a refrigerator at 4 °C for two months to initiate the germination process. During this period, we regularly sprayed water on the soil to maintain its moisture. Subsequently, we moved the seeds to the sediment substrate and put them in an artificial climate chamber to facilitate germination. After a month and a half of growth, when the seedlings reached an average height of about 12 cm, we transferred both the seedlings and the sediment to the flooding devices, with each device accommodating 100 seedlings. The flooding device is one we previously used in other studies (Zhang et al., 2023), the structure of which is shown in Fig. 1. This device consists of two water tanks, an upper tank containing sediment and plants, and a lower tank containing treatment solution. Within the lower tank is a submersible pump used to extract the treatment solution to the upper tank and maintain varying durations of flooding. Subsequently, the treated solution in the upper tank flows back into the lower tank under the force of gravity, completing a flooding cycle. In this process, due to the repeated immersion and withdrawal of the treatment solution from the sediment and plant system, this system simulates the effect of tidal seawater on intertidal sediment in an actual tidal flat environment. These flooding devices were situated in an artificial climate chamber. The climate parameters of the chamber were set as follows: temperature between 28 and 32 °C, humidity maintained at 75

%–80 %, light intensity ranging from 7000 to 14,000 Lux, and a light cycle of 12 h (light) followed by 12 h (dark).

We designed a total of 9 treatment groups, each randomly divided into three sets of flooding devices. Using a factorial experimental design, we aimed to examine how varying flooding durations and salinity levels influence the Fe-OC binding characteristics of sediment in the rhizosphere of *S. mariqueter* and its associated rhizosphere bacteria. Previous research indicated that the seawater salinity near Chongming Dongtan ranged around 15 ppt, with daily average flooding durations ranging from 1.77 h day⁻¹ (at an elevation of 3.7 m) to 17.90 h day⁻¹ (at an elevation of 1.6 m) (Xue et al., 2018b; Li et al., 2020b). In the waters near the Yangtze River Estuary, the salinity ranged from 0 to 34 ppt (Guo et al., 2020). We established three gradients of salinity treatments (0 ppt, 15 ppt, 35 ppt) and three gradients of flooding durations (0 h, 5 h, 10 h), resulting in a total of nine treatment groups. To simulate the semi-diurnal tidal flooding pattern of the Yangtze River Estuary, we conducted two flooding events daily, in the morning and evening. The experimental groups were exposed to flooding durations of 5 h and 10 h, with a flood depth of approximately 5 cm (above the sediment). As for the control group, during each flooding treatment, we maintained a submerged state for 1 min and promptly drained the excess water after fully saturating the soil substrate. We prepared the flooding solutions using NaCl. The experimental period spanned 30 days, during which we regularly replenished tap water every 3 days to prevent water loss in the treatment solutions. The flooding solutions were replaced on a weekly basis. Upon completion of the experiment, we carefully collected rhizosphere sediment within 5 mm of the root surface using sterilized forceps (Phillips and Fahey, 2006). Some portions of the sediment samples were stored in a -80 °C environment for subsequent microbial extraction and sequencing analysis. The remaining samples were freeze-dried, ground, sieved through a 0.15 mm soil sieve, and preserved for subsequent chemical analysis.

2.2. Measurement

2.2.1. Soil physicochemical parameters

Some physicochemical factors of the sediment, such as Eh, pH and electrical conductivity (EC), were measured in situ during the sampling using a portable oxidation-reduction potential meter (FJA-6, Nanjing Chuandi Instrument Equipment Co., Ltd., China) and a portable conductivity meter (Spectrum 2265FS, USA), respectively. Total C (TC),

total nitrogen (TN), and total OC (TOC) in the sediment were measured using an elemental analyzer (Vario Macro, Elementar Analysensysteme GmbH, Germany). Soil particle size was measured using a laser particle-size analyzer (Model LSTM 13320, Beckman Coulter, Inc., USA).

2.2.2. Fe oxides and Fe-OC

In accordance with the methodologies described by Lalonde et al. (2012) and Liu et al. (2020), we employed the following procedures for the extraction of crystalline Fe (hydr-) oxides (Fe_{DH}), amorphous Fe (hydr-) oxides (Fe_{HH}), and organo-metal complexes (Fe_{PP}), as well as their corresponding OC associations (Fe_{DH}-OC, Fe_{HH}-OC, and Fe_{PP}-OC). The extraction reagents used were 0.05 mol L⁻¹ dithionite-HCl, 0.25 M hydroxylamine hydrochloride in 0.25 mol L⁻¹ HCl, and 0.1 mol L⁻¹ sodium pyrophosphate. For each sample, two separate 0.25-g sediment samples were weighed and placed in individual, clean 50-ml centrifuge tubes. One tube received 15 ml of the respective extraction reagent, while the other tube received 15 ml of deionized water as a control. The tubes were then incubated at room temperature and agitated on a shaker at a speed of 160 rpm for 16 h. Following agitation, the tubes were centrifuged at 4000 rpm for 30 min. The resulting supernatant was filtered through a 0.22 μm polyethersulfone membrane to prepare it for the subsequent determination of Fe content. The Fe content in the extraction solution was determined using the o-phenanthroline photometry method (Shyla et al., 2012) (specific measurement procedures are described in the Supplementary Material). The precipitates obtained after extraction were freeze-dried, and their TOC content was measured using an elemental analyzer (Vario Macro, Elementar Analysensysteme GmbH, Germany). The OC content associated with each form of Fe (hydr-) oxide was then calculated using the following equation, as described by Lalonde et al. (2012):

$$Fe - OC = OC_C - OC_E$$

where OC_C and OC_E represent the OC content in the control centrifuge tube and the extraction centrifuge tube, respectively.

The calculation of different forms of Fe-OC is based on the following equation:

$$f_{Fe-OC(DH,HH,PP)}(\%) = \frac{Fe - OC}{TOC} \times 100$$

The sum of the fractions of the three Fe-OC to sediment TOC was calculated as $f_{Fe-OC(T)}$.

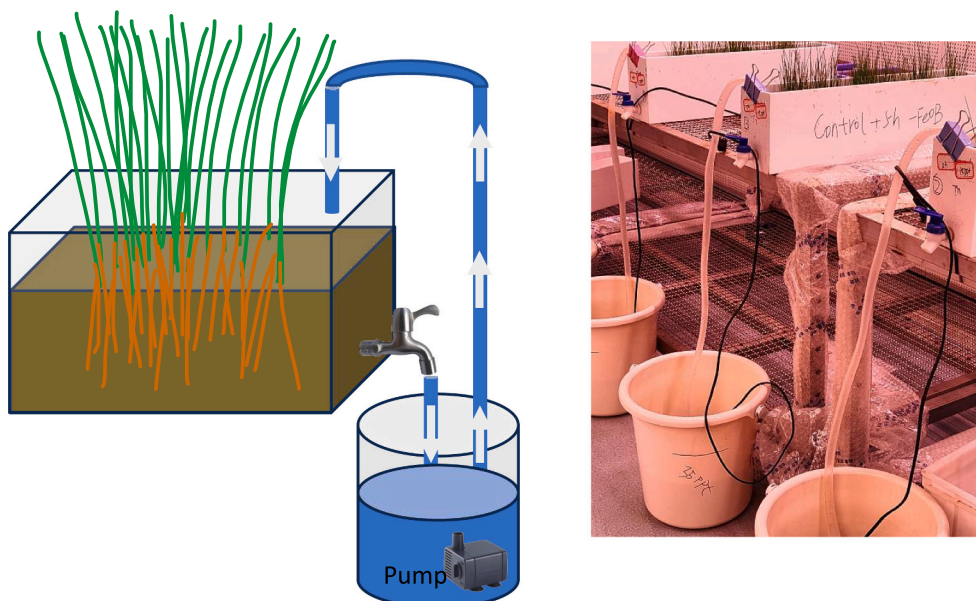


Fig. 1. (A) Diagram of small automatic flooding device, (B) experimental layout, and (C) internal structure.

2.2.3. The weak acid extractable fraction of Fe

The total Fe content in sediments was extracted using the HNO_3 -HF- HClO_4 method (Zang et al., 2017), while the weak acid extractable Fe was extracted using 0.5 mol L^{-1} HCl (Kostka and Luther, 1994). The Fe content of the extract was determined via the o-phenanthroline photometry method (Shyla et al., 2012) (for detailed measurement methods, please refer to the Supplementary material).

2.2.4. Total phenol and polyphenol oxidase

The total phenolic (TP) content of the sediments was determined using the Folin Ciocalteu reagent, following the method described by Siddiqui et al. (2017). The activity of polyphenol oxidase (PPO) in the sediments was measured using the catechol colorimetric method, according to the study by Shao et al. (2008) (for detailed measurement methods, please refer to the Supplementary material).

2.2.5. 16s rDNA sequencing

The sediment samples were transported to Shanghai Majorbio Bio-Pharm Technology Co. on dry ice at low temperatures for the purpose of extracting, amplifying, and sequencing bacterial DNA. The V3-V4 hypervariable region of 16S rDNA was targeted and amplified in each sample using specific polymerase chain reaction (PCR) primers, namely 338F (5'-AACTCCTACGGAGGAGCA-3') and 806R (5'-GAC-TACHVGGTCTCATAT-3'). Subsequently, high-throughput sequencing of the amplified 16S rDNA was performed utilizing the Illumina Miseq PE 300 platform. To examine the species composition and diversity information within the samples, a clustering analysis was conducted on the concatenated and filtered clean tags obtained from all samples, with a similarity threshold set at 97%. This process resulted in the generation of Operational Taxonomic Units (OTUs). Representative sequences from

the OTUs were then selected and compared against a database to acquire species annotation information.

2.3. Statistical analyses

The average and standard deviations (SDs) of triplicate samples were calculated for the physicochemical factors and the content of different fractions of Fe (hydr-) oxides in rhizosphere soils. To investigate potential variations in sediment parameters among different treatment groups, both one-way and two-way analyses of variance (ANOVA) were utilized, along with post hoc multiple comparisons (Tukey's test). Principal Coordinates Analysis (PCoA) was performed on the samples using R software (v3.6.1; R Core Team, 2019) to evaluate their spatial distribution. Moreover, a bar plot depicting the changes in bacterial relative abundance at the phylum level was created using the Vegan and Picante packages.

3. Results

3.1. Soil physicochemical parameters

The sediment has a loamy sand texture, with proportions of silt, clay, and sand being 1.24%, 34.8%, and 63.69%, respectively (Table S1 in the supplementary materials). The EC and Eh of the rhizosphere sediment in *S. mariqueter* were significantly affected by different flooding and salinity treatments. As the duration of flooding increased, the Eh showed a decreasing trend, particularly in the treatment group with 0 ppt salinity (Fig. 2D). The sediment EC increased significantly with higher salinity levels in the treatment solutions (Fig. 2C). There were no significant differences in TOC and C/N among the different treatment

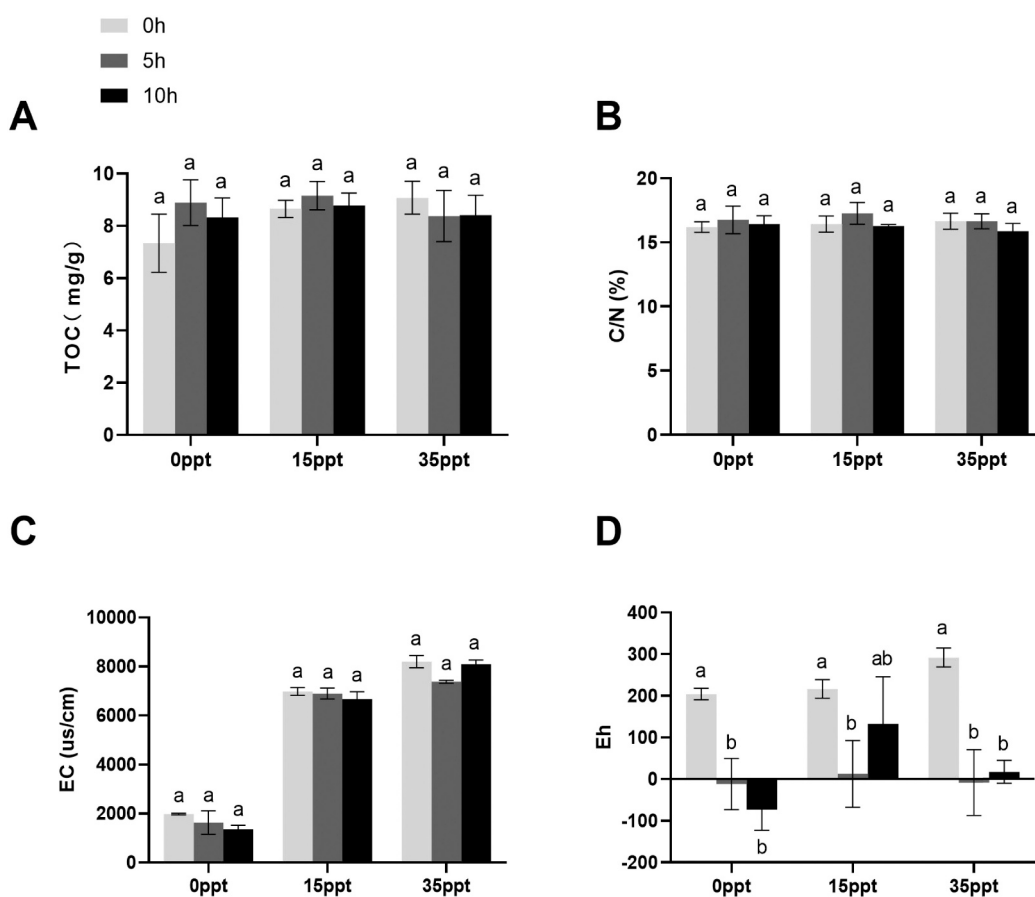


Fig. 2. Changes in (A) TOC, (B) C/N, (C) EC, and (D) Eh of the rhizosphere sediments of *S. mariqueter* under different levels of salinity and flooding treatment. For each salinity gradient, data with different letters are significantly different at $p < 0.05$.

groups (Figs. 2A and B). The sediment TP concentration showed no significant variation among the treatment groups (Fig. S1A). Meanwhile, the activity of PPO noticeably decreased with extended flooding duration in the 0 ppt treatment, while maintaining stability in the other treatment groups (Fig. S1B). Treatments with 15 ppt and 35 ppt salinity significantly lowered the pH of the sediment under 0 h and 5 h flooding treatments compared to 0 ppt (Fig. S1C).

3.2. The weak acid extractable fraction of Fe in the sediment

The results of the two-way ANOVA revealed significant effects of salinity treatment on the content of Fe (II), Fe (III), and the Fe (II)/Fe (III) ratio in the sediment ($p < 0.05$). However, flooding only had a notable impact on the Fe (II) content and the Fe (II)/Fe (III) ratio in the sediment ($p < 0.05$). Additionally, the interaction between salinity and flooding exhibited significant effects on Fe (III) content and the Fe (II)/Fe (III) ratio ($p < 0.05$, Table 1). Under non-flooding conditions (0 h), the content of Fe (II) in the sediment exhibited a significant decline with increasing salinity. However, as the flooding duration extended (5 h and 10 h), this trend became less evident (Fig. 3A). Irrespective of the flooding duration, salinity did not significantly influence the content of Fe (III) in the sediment (Fig. 3B). In varying flooding conditions, the Fe (II)/Fe (III) ratio demonstrated a similar trend to that of the Fe (II) content, decreasing with rising salinity, particularly during 5 h of flooding (Fig. 3C).

3.3. Fe oxides and Fe bound-OC content

The results of the two-way ANOVA revealed significant effects of flooding on Fe_{DH} and Fe_{PP} ($p < 0.5$), while salinity had a significant effect on Fe_{PP} ($p < 0.5$). Moreover, there was a significant interaction between salinity and flooding with respect to Fe_{HH} content ($p < 0.5$) (Table 1). Overall, the variations in Fe_{DH} and Fe_{HH} content in response to different salinity and flooding conditions were not pronounced. Under the 0 h flooding treatment, both Fe_{DH} and Fe_{HH} showed significantly higher values in the control group (0 ppt) compared to the high salinity group (35 ppt) (Figs. 4A and B). As the flooding duration increased, the content of Fe_{DH} showed an increase in both the 15 ppt and 35 ppt treatment groups, but the differences between the groups were not significant (Fig. 4A). Conversely, Fe_{PP} displayed a more evident trend under varying flooding and salinity treatments. Under the 10 h flooding treatment, Fe_{PP} content was significantly higher in the 15 ppt treatment group compared to the 35 ppt treatment group. Additionally, under high salinity conditions (35 ppt), Fe_{PP} content significantly decreased with increasing flooding duration ($p < 0.05$) (Fig. 4C).

The response of different forms of Fe oxide-bound OC content varies under the influence of flooding and salinity. The two-way ANOVA

Table 1

Two-way ANOVA showing the effect of salinity and flooding time on different measured parameters of rhizosphere sediments of *S. maritimum* (the DF of interaction, salinity and waterlogging are 4,2 and 2).

Source of variations	Flooding		Salinity		Flooding*salinity	
	MS	p Value	MS	p Value	MS	p Value
TOC	0.481	0.447	1.077	0.181	1.023	0.175
C/N	1.121	0.108	0.171	0.685	0.280	0.645
Fe_{DH}	0.397	<0.05	0.131	0.248	0.105	0.341
Fe_{HH}	0.048	0.310	0.021	0.585	0.180	<0.01
Fe_{PP}	0.007	<0.001	0.002	<0.01	0.001	0.157
Fe_{DH-OC}	0.039	0.490	0.606	<0.001	0.212	<0.05
Fe_{HH-OC}	0.074	0.576	0.011	0.918	0.027	0.932
Fe_{PP-OC}	0.331	<0.01	0.053	0.377	0.088	0.188
Fe(II)	112.558	<0.05	159.499	<0.05	58.396	0.065
Fe(III)	0.000	0.976	0.077	<0.05	0.072	<0.01
Fe(II)/Fe(III)	0.016	<0.01	0.037	<0.001	0.012	<0.01
T-Phenol	0.273	<0.01	0.004	0.879	0.090	0.059

results demonstrated that flooding had a significant impact on Fe_{PP-OC} ($p < 0.5$), while salinity had a significant effect on Fe_{DH-OC} ($p < 0.05$). Moreover, there was a significant interaction between salinity and flooding in relation to Fe_{DH-OC} ($p < 0.05$) (Table 1). Under high salinity treatment (35 ppt), the content of Fe_{DH-OC} increased with the duration of flooding, while the content of Fe_{PP-OC} decreased ($p < 0.05$) (Figs. 4D and F). For the 0 h flooding treatment, the application of high salinity (35 ppt) significantly amplified the Fe_{PP-OC} content ($p < 0.05$) (Fig. 4F), while the Fe_{DH-OC} content peaked under the 15 ppt treatment ($p < 0.05$) (Fig. 4D). There were no significant differences in Fe_{HH-OC} content among the treatment groups (Fig. 4E).

The patterns of f_{Fe-OC} variation align with Fe-OC. In the presence of high salinity treatment (35 ppt), increasing flooding duration led to an elevation of $f_{Fe-OC(DH)}$ and a reduction of $f_{Fe-OC(PP)}$ ($p < 0.05$) (Figs. S2A and C). However, $f_{Fe-OC(HH)}$ showed no significant differences among the flooding treatment groups (Fig. S3B). Assessing the proportion of Fe-OC relative to TOC in the sediment, approximately 20.24 % to 48.28 % of TOC was associated with iron oxides. Nevertheless, there were no significant differences in $f_{Fe-OC(T)}$ among the treatment groups (Fig. S2D). The OC:Fe molar ratio for the three forms of iron (hydr-)oxides is illustrated in Fig. 5. Overall, OC:Fe-DH and OC:Fe-HH were approximately 1, while OC:Fe-PP exceeded 20, indicating a significantly higher ratio than that of OC:Fe-DH and OC:Fe-HH.

3.4. Difference in the diversity and structure of the bacteria community

The PCoA analysis showed that the first two coordinates explained 59.22 % of the differences in bacterial communities under the treatments (Fig. 6). The bacterial communities differed notably across treatments with varying salinity gradients, particularly between the 0 ppt treatment and the 15 ppt and 35 ppt salinity treatments (Fig. 6). In the 15 ppt treatment group, the distance of the 10 h flooding treatment was notably greater when compared to 0 h and 5 h, suggesting that the 10 h flooding had a more profound impact on the bacterial community structure in this particular treatment group. In contrast, the 0 ppt and 35 ppt salinity treatment groups exhibited a notable difference between the 0 h flooding treatment and the 5 h and 10 h flooding treatment, indicating a heightened influence of flooding on the bacterial community structure in these groups (Fig. 6).

3.5. Correlation between Fe redox cycling bacteria and sediment physicochemical factors

Regarding the relative abundance of several typical FeRB, *Deferri-soma* notably increased with longer flooding duration in the high salinity treatment group (35 ppt) ($p < 0.05$) (Fig. 7A). Similarly, *Geothermobacter* demonstrated a similar trend, with the lowest relative abundance in the 15 ppt treatment group ($p < 0.05$) (Fig. 7B). On the other hand, FeOB like *Paracoccus* and *Pseudomonas* notably decreased with prolonged flooding duration ($p < 0.05$) and exhibited a declining trend with higher salinity levels (Figs. 7D and E). The two-way ANOVA results indicated that both flooding and salinity treatments significantly impacted the overall relative abundance of FeRB, with significant interactive effects on the relative abundance of *Geothermobacter* and *Shewanella* ($p < 0.05$) (Table S2). Salinity had a highly significant impact on the relative abundance of root-associated *Deferri-soma* ($p < 0.001$) (Table S2). Furthermore, salinity had a more substantial influence on the relative abundance of FeOB, with significant effects observed on the relative abundance of *Paracoccus* and *Pseudomonas* ($p < 0.001$). The interaction between flooding and salinity significantly affected *unclassified_f_Gallionellaceae* ($p < 0.01$) (Table S2), while flooding alone did not have a significant impact on the relative abundance of FeOB.

4. Discussion

The biomass of salt marsh plants in tidal flat wetlands is a significant

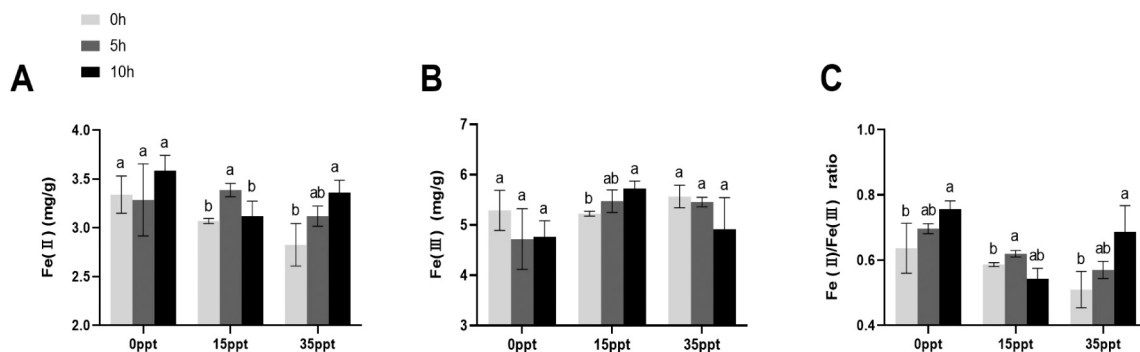


Fig. 3. Changes in Fe(II), Fe(III) content and Fe(II)/Fe(III) ratio of the rhizosphere sediments of *S. mariqueter* under different levels of salinity and flooding treatment. For each salinity gradient, data with different letters are significantly different at $p < 0.05$.

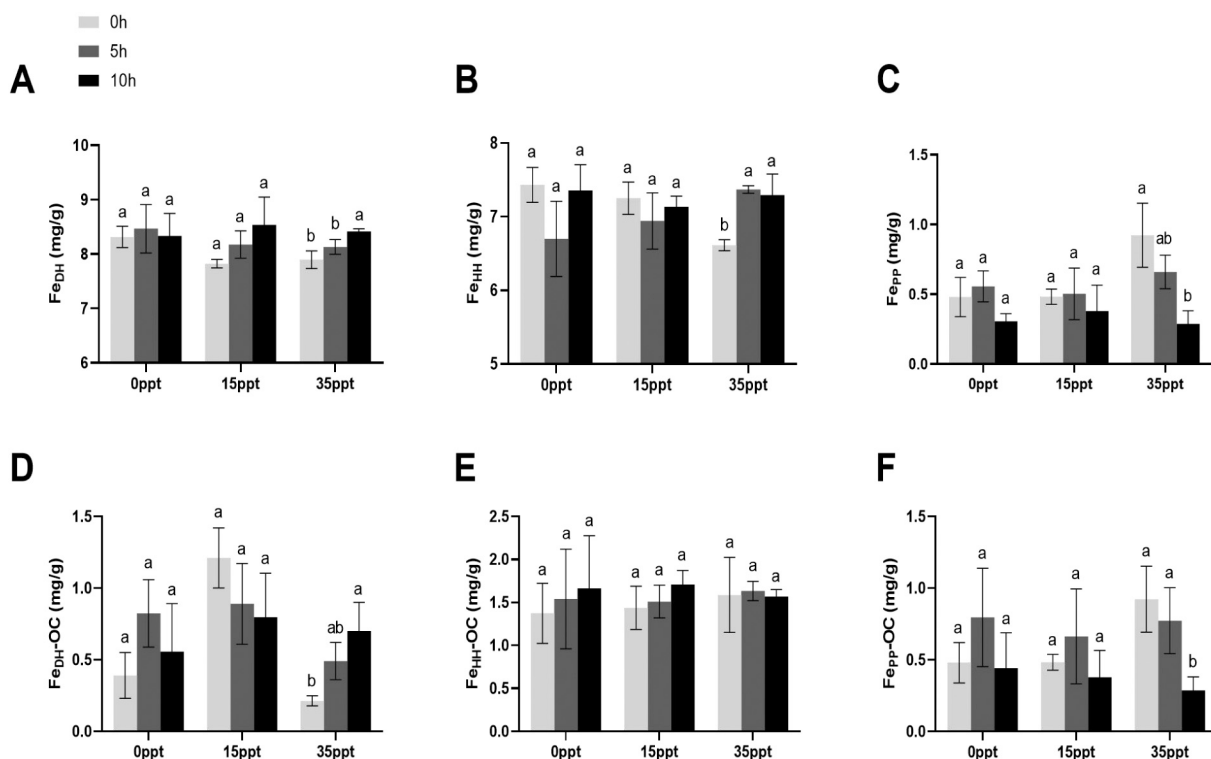


Fig. 4. Changes in (A) Fe_{DH} (B) Fe_{HH} (C) Fe_{PP} (D) Fe_{DH-OC} (E) Fe_{HH-OC} and (F) Fe_{PP-OC} content of the rhizosphere sediments of *S. mariqueter* under different levels of salinity and flooding treatment. For each salinity gradient, data with different letters are significantly different at $p < 0.05$.

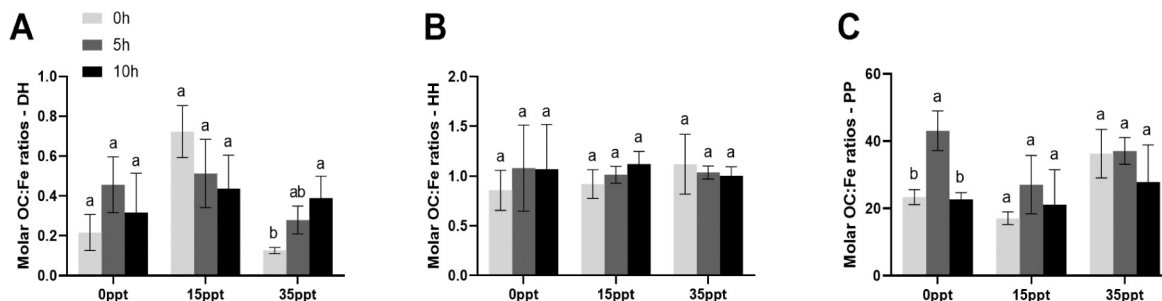


Fig. 5. Variations of molar OC:Fe ratios in the rhizosphere sediments of *S. mariqueter*. For each salinity gradient, data with different letters are significantly different at $p < 0.05$.

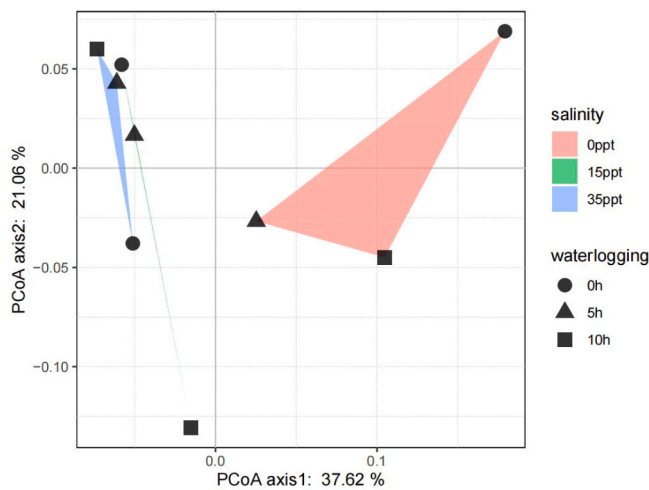


Fig. 6. Principal Coordinate Analyses (PCoA) analysis of the bacterial community in rhizosphere sediments of *S. mariqueter*.

source of sediment OC (De Deyn et al., 2008). Increased waterlogging and salt stress may impact vegetation development (Medeiros et al., 2013), leading to decreased plant biomass (Xue et al., 2018a) and alterations in root exudation processes (Henry et al., 2007; Xie et al., 2020), thereby affecting the input of plant-derived C into sediment and the storage of OC. Generally, the increase in intertidal sediment salinity corresponds to a reduction in sediment TOC content. However, our study revealed that the application of different levels of salinity and flooding treatments did not significantly affect the TOC content in the rhizosphere of *S. mariqueter* (Fig. 2). These findings are in accordance with the research conducted by Xue et al. (2020), where they observed a strong negative correlation between plant biomass of *S. mariqueter* and salinity following four months of exposure to diverse salinities (0 to 35 ppt), while the OC content in the sediment remained relatively stable. In contrast, Bai et al. (2021) found in the intertidal wetlands of the Minjiang Estuary that as salinity increased, plant biomass decreased, leading to a reduction in sediment OC storage. These differences could be attributed to various factors, including changes in sediment texture and vegetation distribution patterns, as well as variations in flooding and salinity conditions in different intertidal habitats. Intertidal wetlands exhibit stronger adaptability to changes in flooding and salinity conditions compared to freshwater wetlands (Chambers et al., 2013). Thus, short-term changes in flooding and salinity conditions may not immediately impact sediment OC levels, as the sequestration of OC is a relatively slow process. However, long-term observations indicate that changes in flooding and salinity do indeed significantly affect OC storage in sediments (Jiang et al., 2015).

The crystallinity and valence state transition of sediment Fe can be impacted by changes in sediment redox states (Doran et al., 2006; Hyun et al., 2009; Yu, 2018). In this study, flooding treatment raised the Fe (II)/Fe (III) ratio while considerably reducing sediment redox potential (Fig. 2D). This shows that the treatment of flooding increases the anaerobic stress on the sediment, which causes the sediment to lose more Fe (III). According to Liu et al. (2020), the Fe (II) produced by the reduction of Fe (III) in sediment can be reoxidized to create amorphous Fe (hydr-) oxides. Because of this, increasing flooding stress frequently results in a reduction in the crystallinity of sedimentary Fe (hydr-) oxides and an increase in the proportion of amorphous Fe (hydr-) oxides (Darke and Walbridge, 2000; Zhang et al., 2003). The findings of this investigation support the findings above. In the flooding groups (5 h and 10 h) under the high salinity treatment (35 ppt), the amount of amorphous Fe (hydr-) oxides (Fe_{HH}) was substantially greater than that in the 0 h group (Fig. 4B). This shows that the flooding treatment greatly enhanced the amount of amorphous Fe (hydr-) oxides in the rhizosphere

of *S. mariqueter* under high salinity conditions. The levels of crystalline Fe (hydr-) oxides (Fe_{DH}) in the rhizosphere of *S. mariqueter* were significantly lower in the 15 and 35 ppt salinity treatments compared to the 0 ppt treatment (Fig. 4A), indicating that the presence of salt stress resulted in a significant decrease in the content of crystalline Fe (hydr-) oxides. Previous studies have indicated that FeRB and FeOB play significant roles in the formation and decomposition of Fe (hydr-) oxides in the rhizosphere of wetland plants. The amorphous Fe (hydr-) oxides serve as the primary electron acceptors for FeRB and are the primary products of FeOB activity (Lovley, 1991; Weiss et al., 2003). In this study, however, our results demonstrate that the relative abundance of certain FeRB in the *S. mariqueter* rhizosphere, such as *Deferrisoma* and *Geothemobacter*, exhibits a similar trend of variation with changing salinity as that of amorphous Fe (hydr-) oxides, increasing with increasing salinity. Conversely, the relative abundance of typical FeOB, such as *Paracoccus* and *Pseudomonas*, displays a trend similar to that of crystalline Fe (hydr-) oxides, generally decreasing with increasing salinity. These results suggest that Fe redox cycling bacteria are not the primary driving forces for the formation and transformation of Fe (hydr-) oxides in the *S. mariqueter* rhizosphere, although the results of the principal coordinate analysis (PCoA) indicate that flooding and salinity indeed significantly influence the structure and diversity of *S. mariqueter* rhizospheric sediments (Fig. 6 and Table S3).

In this study, the pH values in the salinity treatment groups (15 ppt and 35 ppt) were substantially lower than those in the control group ($p < 0.05$) during the 0-h flooding treatment (Fig. S1C). These results suggest that the significant decrease in the content of crystalline Fe (hydr-) oxides under salt treatment may be the result of the decreased pH of the treatment solution. Previous research has shown that salt stress and floods can modify the quantity and composition of plant REs, hence affecting rhizosphere pH (Henry et al., 2007; Ding et al., 2014). Citric acid and oxalic acid concentrations in rice REs were found to be considerably higher under salt stress, according to Ding et al. (2014). It has been demonstrated that the amount of short-range-order minerals in sediments decreases substantially when the amount of oxalic acid in REs increases (Keilweit et al., 2015). In addition, the initial oxidation products of Fe (II) are mostly weakly crystalline Fe (hydr-) oxides, which subsequently transform into higher crystallinity Fe (hydr-) oxides under stable oxidizing conditions (Vogelsang et al., 2016). Although this study did not track and measure plant growth indicators, most relevant studies indicate that salt stress can lead to slowed plant growth and weakened root ROL processes (Cheng et al., 2012; Reddy et al., 2017), which can interfere with the crystallization process of rhizosphere Fe (hydr-) oxides, resulting in a significant decrease in the content of crystalline Fe (hydr-) oxides.

Changes in flooding and salinity conditions impact not only the cycling and transformation of sediment Fe (hydr-) oxides but also the coupling mode between sediment Fe (hydr-) oxides and OC. Fe (hydr-) oxides and OC can bind to one another in sediment by either adsorption or co-precipitation. Adsorption is the process by which OC and Fe (hydr-) oxide surface groups exchange ligands to create Fe-OC complexes, whereas co-precipitation is the process by which Fe (hydr-) oxides and OC establish strong covalent bonds to generate insoluble organic ligands. In contrast to co-precipitation, which may contain a larger concentration of OC than adsorption (Wagai and Mayer, 2007; Barber et al., 2017), adsorption has an OC:Fe molar ratio that is typically around 1. In this study, OC:Fe-HH was much higher than OC:Fe-DH, demonstrating that Fe_{HH} has a greater potential for sediment OC adsorption than Fe_{DH} (Fig. 5A). According to Liu et al. (2020), whereas Fe_{PP} mostly binds OC by co-precipitation, Fe_{DH} primarily does so through adsorption. Similar results were found in this investigation, where the ratios of OC:Fe-DH and OC:Fe-HH were close to 1, showing that Fe_{DH} and Fe_{HH} bind OC by adsorption, whereas the ratio of OC:Fe-PP was >20 , indicating that Fe_{PP} binds OC through co-precipitation. In this study, prolonged flooding (10 h) and high salinity treatment (35 ppt) significantly increased the content of Fe_{DH} -OC, while the content of Fe_{PP} -OC decreased

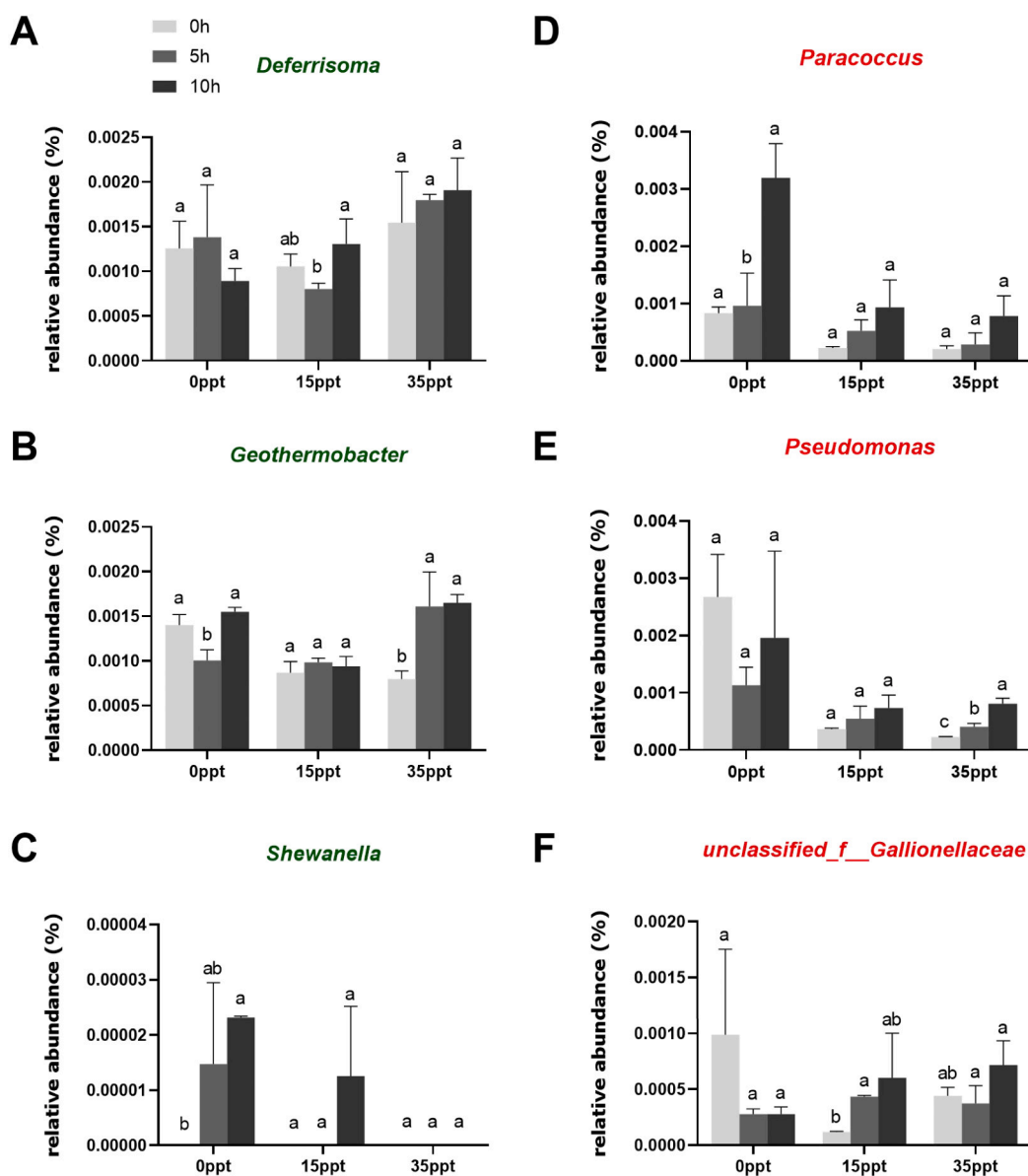


Fig. 7. Relative abundance of the selected dominant FeRB (A, B, and C) and FeOB (D, E, and F) genera in rhizosphere of *S. mariqueter*. For each salinity gradient, data with different letters are significantly different at $p < 0.05$.

significantly (Fig. 4D and F), indicating that intensified water-salt stress promotes the adsorption of sediment Fe (hydr-) oxides to OC and inhibits their coprecipitation. This inference is supported by the variation in the sediment OC:Fe molar ratio, where prolonged flooding (10 h) and high salinity treatment (35 ppt) significantly increased the OC:Fe-DH ratio, demonstrating a significant enhancement in the adsorption capacity of OC by Fe_{DH} . A noteworthy point is that the increase in seawater salinity also leads to an increase in the ionic strength, including ions such as sodium, sulfur, magnesium, and calcium. These ions compete with OC for binding sites on the surface of Fe (hydr-) oxides, thereby affecting the adsorption of OC by Fe (hydr-) oxides (Tomaszewski et al., 2021). The competitive binding mechanism of OC and seawater ions with Fe (hydr-) oxides warrants further investigation in the future.

Soil pH serves as a critical determinant affecting the solubility of soil Fe minerals, the composition of soil organic matter, and the interaction between Fe (hydr-) oxides and OC within the soil (Ghazali et al., 2020; Wang et al., 2023). Within sediment, pH is primarily shaped by sediment characteristics, including clay content, oxide content, and organic matter content (Delgado and Gomez, 2016). Sediment moisture content

and salinity have also been proven to impact sediment pH (Ghazali et al., 2020). In this study, an evident decrease in sediment pH was observed with the increase in salinity ($p < 0.05$) (Fig. S1C). Similar findings were reported by Ghazali et al. (2020), who observed a notable decline in the pH of paddy soil as salinity levels increased. Fe (hydr-) oxides often bind to OC in sediment at lower pH levels primarily by complexation and coprecipitation, but at higher pH levels, adsorption takes over (Chen et al., 2014; Liu et al., 2020). Fe (hydr-) oxides in the rhizosphere sediment of *S. mariqueter* largely bind to OC by adsorption, according to this study's finding that $f_{Fe-OC(PP)}$ is lower than the total of $f_{Fe-OC(DH)}$ and $f_{Fe-OC(HH)}$ (Fig. S2). This might be explained by the sediment's greater levels of Fe_{DH} and Fe_{HH} , and earlier research has shown that Fe_{DH} content is the most significant influencing factor for Fe_{DH} -OC concentration (Liu et al., 2020). Under intensified flooding and salt stress, $f_{Fe-OC(PP)}$ decreases significantly while $f_{Fe-OC(DH)}$ increases, indicating that intensified flooding and salt stress promote the adsorption of Fe (hydr-) oxides to OC in *S. mariqueter* rhizosphere sediment, inhibiting coprecipitation processes. Notably, $f_{Fe-OC(HH)}$ is significantly higher than $f_{Fe-OC(DH)}$ (Fig. S2), despite the fact that the content of Fe_{HH} is

significantly lower than Fe_{DH} in all treatment groups (Fig. 3). This is because amorphous Fe (hydr-) oxides has a higher specific surface area and a stronger capacity to adsorb OC (Chen et al., 2020; Coward et al., 2017).

Amid different flooding and salt treatments, $f_{Fe-OC(T)}$ showed minimal changes (Fig. S2D), consistent with the trends observed in TOC response across various flooding and salinity levels. As previously mentioned, short-term fluctuations in water-salt conditions do not exert a significant influence on the TOC content in the intertidal wetlands. Considering the primary results of this research, the levels of sediment Fe (hydr-) oxides can be considered relatively steady. With both OC and Fe (hydr-) oxide content being crucial factors impacting Fe-OC levels, their relatively stable statuses contribute to the lack of substantial alterations in the overall sedimentary Fe (hydr-) oxides and OC content across the treatment groups. Consequently, this lack of variation does not impact the proportion of OC that is bound by Fe (hydr-) oxides in the TOC. Although $f_{Fe-OC(T)}$ demonstrates remarkable stability in response to water-salt changes, data on the proportion of OC bound by Fe (hydr-) oxides to the TOC indicate that prolonged flooding time and high salinity increase $f_{Fe-OC(DH)}$ and decrease $f_{Fe-OC(PP)}$ (Figs. S2A and D). This implies that a greater amount of OC is bound by highly crystalline Fe (hydr-) oxides, making this portion of OC less accessible to microorganisms compared to the OC bound by amorphous Fe (hydr-) oxides (Lovley and Phillips, 1986), thus exhibiting higher stability.

5. Conclusion

This study revealed that heightened flooding and elevated salt stress led to an increase in the proportion of amorphous Fe (hydr-) oxides within sediment, coupled with a reduction in the quantity of crystalline Fe (hydr-) oxides. This combination resulted in an overall decline in the crystalline nature of sediment Fe (hydr-) oxides. Moreover, prolonged flooding and exposure to high salt levels hindered the bonding of complexed Fe (hydr-) oxides (Fe_{PP}) to OC. As a consequence, a greater amount of OC became associated with crystalline Fe (hydr-) oxides (Fe_{DH}). Additionally, under these conditions, there was a boost in the adsorption of Fe (hydr-) oxides to OC, while the co-precipitation processes were suppressed. These findings underscore the impact of water and salt stress on the interaction between sediment Fe (hydr-) oxides and OC within the rhizosphere of *S. maritima*. Importantly, despite the alterations in the environment, the short-term stability of the Fe-OC pool remained evident. To comprehensively understand the implications of heightened flooding and salt stress, future investigations should delve into the lasting changes affecting the dynamics of the sediment Fe-OC pool, along with the role of Fe-OC in the sequestration of sediment OC.

CRedit authorship contribution statement

Yuxin Bi: Investigation, Writing – original draft, Formal analysis. **Xiaoqing Gao:** Investigation, Resources. **Lin Su:** Investigation, Resources. **Ying Lei:** Investigation, Visualization. **Tianyou Li:** Investigation, Formal analysis. **Xinhan Dong:** Investigation, Resources. **Xiuzhen Li:** Supervision. **Zhongzheng Yan:** Conceptualization, Supervision, Writing – review & editing.

Declaration of competing interest

The authors declare that they have no known competing financial interests or personal relationships that could have appeared to influence the work reported in this paper.

Data availability

Data will be made available on request.

Acknowledgement

The work described in this paper was supported by the Key Projects of National Natural Science Foundation of China [grant number 42141016] and National Natural Science Foundation of China [grant number 41877413].

Appendix A. Supplementary data

Supplementary data to this article can be found online at <https://doi.org/10.1016/j.scitotenv.2023.168447>.

References

- Bai, J., Luo, M., Yang, Y., Xiao, S., Zhai, Z., Huang, J., 2021. Iron-bound carbon increases along a freshwater–oligohaline gradient in a subtropical tidal wetland. *Soil Biol. Biochem.* 154, 108128 <https://doi.org/10.1016/j.soilbio.2020.108128>.
- Barber, A., Brandes, J., Leri, A., Lalonde, K., Balind, K., Wirick, S., Wang, J., Gélinas, Y., 2017. Preservation of organic matter in marine sediments by inner-sphere interactions with reactive iron. *Sci. Rep.-UK* 7 (1), 366. <https://doi.org/10.1038/s41598-017-00494-0>.
- Bertin, C., Yang, X., Weston, L.A., 2003. The role of root exudates and allelochemicals in the rhizosphere. *Plant Soil* 256 (1), 67–83. <https://doi.org/10.1023/a:1026290508166>.
- Canarini, A., Mariotte, P., Ingram, L., Merchant, A., Dijkstra, F.A., 2018. Mineral-associated soil carbon is resistant to drought but sensitive to legumes and microbial biomass in an Australian grassland. *Ecosystems* 21 (2), 349–359. <https://doi.org/10.1007/s10021-017-0152-x>.
- Chambers, L.G., Osborne, T.Z., Reddy, K.R., 2013. Effect of salinity-altering pulsing events on soil organic carbon loss along an intertidal wetland gradient: a laboratory experiment. *Biogeochemistry* 115 (1), 363–383. <https://doi.org/10.1007/s10533-013-9841-5>.
- Chapman, S.K., Hayes, M.A., Kelly, B., Langley, J.A., 2019. Exploring the oxygen sensitivity of wetland soil carbon mineralization. *Biol. Lett.* 15 (1), 20180407. <https://doi.org/10.1098/rsbl.2018.0407>.
- Chen, C., Dynes, J.J., Wang, J., Sparks, D.L., 2014. Properties of Fe-organic matter associations via coprecipitation versus adsorption. *Environ. Sci. Technol.* 48 (23), 13751–13759. <https://doi.org/10.1021/es503669u>.
- Chen, C., Meile, C., Wilmoth, J., Barcellos, D., Thompson, A., 2018. Influence of pO₂ on iron redox cycling and anaerobic organic carbon mineralization in a humid tropical forest soil. *Environ. Sci. Technol.* 52 (14), 7709–7719. <https://doi.org/10.1021/acs.est.8b01368>.
- Chen, C., Hall, S.J., Coward, E., Thompson, A., 2020. Iron-mediated organic matter decomposition in humid soils can counteract protection. *Nat. Commun.* 11 (1), 2255. <https://doi.org/10.1038/s41467-020-16071-5>.
- Cheng, H., Wang, Y.S., Ye, Z.H., Chen, D.T., Wang, Y.T., Peng, Y.L., Wang, L.Y., 2012. Influence of N deficiency and salinity on metal (Pb, Zn and Cu) accumulation and tolerance by *Rhizophora stylosa* in relation to root anatomy and permeability. *Environ. Pollut.* 164, 110–117. <https://doi.org/10.1016/j.envpol.2012.01.034>.
- Coward, E.K., Thompson, A.T., Plante, A.F., 2017. Iron-mediated mineralogical control of organic matter accumulation in tropical soils. *Geoderma* 306, 206–216. <https://doi.org/10.1016/j.geoderma.2017.07.026>.
- Coward, E.K., Ohno, T., Plante, A.F., 2018. Adsorption and molecular fractionation of dissolved organic matter on iron-bearing mineral matrices of varying crystallinity. *Environ. Sci. Technol.* 52 (3), 1036–1044. <https://doi.org/10.1021/acs.est.7b04953>.
- Darke, A.K., Walbridge, M.R., 2000. Al and Fe biogeochemistry in a floodplain forest: implications for P retention. *Biogeochemistry* 51 (1), 1–32. <https://doi.org/10.1023/A:1006302600347>.
- De Deyn, G.B., Cornelissen, J.H.C., Bardgett, R.D., 2008. Plant functional traits and soil carbon sequestration in contrasting biomes. *Ecol. Lett.* 11 (5), 516–531. <https://doi.org/10.1111/j.1461-0248.2008.01164.x>.
- Delgado, A., Gomez, J.A., 2016. The soil. Physical, chemical and biological properties. In: Fereres, F.J., Villalobos E. (Ed.), *Principles of Agronomy for Sustainable Agriculture*. Springer International Publishing AG, pp. 15–26.
- Ding, H., Wen, D., Fu, Z., Qian, H., 2014. The secretion of organic acids is also regulated by factors other than aluminum. *Environ. Monit. Assess.* 186 (2), 1123–1131. <https://doi.org/10.1007/s10661-013-3443-5>.
- Doran, G., Eberbach, P., Helliwell, S., 2006. The impact of rice plant roots on the reducing conditions in flooded rice soils. *Chemosphere* 63 (11), 1892–1902. <https://doi.org/10.1016/j.chemosphere.2005.10.027>.
- Gartzia-Bengoetxea, N., Virto, I., Arias-González, A., Enrique, A., Fernández-Ugalde, O., Barré, P., 2020. Mineral control of organic carbon storage in acid temperate forest soils in the Basque Country. *Geoderma* 358, 113998. <https://doi.org/10.1016/j.geoderma.2019.113998>.
- Ghazali, M.F., Wikantika, K., Harto, A.B., Kondoh, A., 2020. Generating soil salinity, soil moisture, soil pH from satellite imagery and its analysis. *Inf. Process. Agric.* 7 (2), 294–306. <https://doi.org/10.1016/j.inpa.2019.08.003>.
- Guo, Y., Rong, Z., Chi, Y., Li, X., Na, R., 2020. The modeling study of interannual variability of Changjiang River plume in summer season. *Trans. Oceanol. Limnol.* 4, 30–41 (in Chinese with English abstract).

- Henry, A., Doucette, W., Norton, J., Bugbee, B., 2007. Changes in crested wheatgrass root exudation caused by flood, drought, and nutrient stress. *J. Environ. Qual.* 36 (3), 904–912. <https://doi.org/10.2134/jeq2006.0425sc>.
- Hopkinson, C.S., Cai, W.J., Hu, X., 2012. Carbon sequestration in wetland dominated coastal systems—a global sink of rapidly diminishing magnitude. *Curr. Opin. Environ. Sustain.* 4 (2), 186–194. <https://doi.org/10.1016/j.cosust.2012.03.005>.
- Huang, X.Q., Tong, C., Luo, M., Yang, Y., Tan, F.F., Pan, Z.Y., Huang, J.F., Liu, N., Chen, X., 2022. Soil organic carbon storage, active component contents, and stability along a flooding gradient in the tidal wetland of the Jiulong River Estuary. *Huanjing Kexue* 43 (4), 2226–2236 (in Chinese with English abstract).
- Hyun, J.H., Mok, J.S., Cho, H.Y., Kim, S.H., Lee, K.S., Kostka, J.E., 2009. Rapid organic matter mineralization coupled to iron cycling in intertidal mud flats of the Han River estuary, Yellow Sea. *Biogeochemistry* 92 (3), 231–245. <https://doi.org/10.1007/s10533-009-9287-y>.
- Jiang, J.Y., Huang, X., Li, X.Z., Yan, Z.Z., Li, X.Z., Ding, W.H., 2015. Soil organic carbon storage in tidal wetland and its relationships with soil physico-chemical factors: a case study of Dongtan of Chongming, Shanghai. *J. Ecol. Rural Environ.* 31 (4), 540–547 (in Chinese with English abstract).
- Kaplan, D.I., Kukkadapu, R., Seaman, J.C., Arey, B.W., Dohnalkova, A.C., Buettner, S., Li, D., Varga, T., Scheckel, K.G., Jaffé, P.R., 2016. Iron mineralogy and uranium-binding environment in the rhizosphere of a wetland soil. *Sci. Total Environ.* 569–570, 53–64. <https://doi.org/10.1016/j.scitotenv.2016.06.120>.
- Keillweit, M., Bougoure, J.J., Nico, P.S., Pett-Ridge, J., Weber, P.K., Kleber, M., 2015. Mineral protection of soil carbon counteracted by root exudates. *Nat. Clim. Chang.* 5 (6), 588–595. <https://doi.org/10.1038/nclimate2580>.
- Kirwan, M.L., Megonigal, J.P., 2013. Tidal wetland stability in the face of human impacts and sea-level rise. *Nature* 504 (7478), 53–60. <https://doi.org/10.1038/nature12856>.
- Kirwan, M.L., Temmerman, S., Skeehan, E.E., Guntenspergen, G.R., Fagherazzi, S., 2016. Overestimation of marsh vulnerability to sea level rise. *Nat. Clim. Chang.* 6 (3), 253–260. <https://doi.org/10.1038/nclimate2909>.
- Kleber, M., Sollins, P., Sutton, R., 2007. A conceptual model of organo-mineral interactions in soils: self-assembly of organic molecular fragments into zonal structures on mineral surfaces. *Biogeochemistry* 85 (1), 9–24. <https://doi.org/10.1007/s10533-007-9103-5>.
- Kögel-Knabner, I., Guggenberger, G., Kleber, M., Kandeler, E., Kalbitz, K., Scheu, S., Eusterhues, K., Leinweber, P., 2008. Organo-mineral associations in temperate soils: integrating biology, mineralogy, and organic matter chemistry. *J. Plant Nutr. Soil Sci.* 171, 61–82. <https://doi.org/10.1002/jpln.200700048>.
- Kostka, J.E., Luther, G.W., 1994. Partitioning and speciation of solid phase iron in saltmarsh sediments. *Geochim. Cosmochim. Acta* 58 (7), 1701–1710. [https://doi.org/10.1016/0016-7037\(94\)90531-2](https://doi.org/10.1016/0016-7037(94)90531-2).
- Lalonde, K., Mucci, A., Ouellet, A., Gelinis, Y., 2012. Preservation of organic matter in sediments promoted by iron. *Nature* 483, 198–200. <https://doi.org/10.1038/nature10855>.
- Li, S., Chen, S., Wang, M., Lei, X., Zheng, H., Sun, X., Wang, L., Han, Y., 2020a. Iron fractions responsible for the variation of Cd bioavailability in paddy soil under variable pe+pH conditions. *Chemosphere* 251, 126355. <https://doi.org/10.1016/j.chemosphere.2020.126355>.
- Li, S.H., Ge, Z.M., Tan, L.S., Hu, M.Y., Li, Y.L., Li, X.Z., Ysebaert, T., 2020b. Morphological and reproductive responses of coastal pioneer sedge vegetation to inundation intensity. *Estuar. Coast. Shelf Sci.* 244, 106945. <https://doi.org/10.1016/j.ecss.2020.106945>.
- Liu, R., Ma, T., Lin, C., Chen, J., Lei, K., Liu, X., Qiu, W., 2020. Transfer and transformation mechanisms of Fe bound-organic carbon in the aquitard of a lake-wetland system during reclamation. *Environ. Pollut.* 263, 114441. <https://doi.org/10.1016/j.envpol.2020.114441>.
- Lovelock, C.E., Duarte, C.M., 2019. Dimensions of Blue Carbon and emerging perspectives. *Biol. Lett.* 15 (3), 20180781. <https://doi.org/10.1098/rsbl.2018.0781>.
- Lovley, D.R., 1991. Dissimilatory Fe(III) and Mn(IV) reduction. *Microbiol. Rev.* 55 (2), 259–287. <https://doi.org/10.1128/mr.55.2.259-287.1991>.
- Lovley, D.R., Phillips, E.J.P., 1986. Organic matter mineralization with reduction of ferric iron in anaerobic sediments. *Appl. Environ. Microbiol.* 51 (4), 683–689. <https://doi.org/10.1128/aem.51.4.683-689.1986>.
- Lyu, H., Watanabe, T., Kilasara, M., Hartono, A., Funakawa, S., 2021. Soil organic carbon pools controlled by climate and geochemistry in tropical volcanic regions. *Sci. Total Environ.* 761, 143277. <https://doi.org/10.1016/j.scitotenv.2020.143277>.
- Medeiros, D.L., White, D.S., Howes, B.L., 2013. Replacement of *Phragmites australis* by *Spartina alterniflora*: the role of competition and salinity. *Wetlands* 33 (3), 421–430. <https://doi.org/10.1007/s13157-013-0400-6>.
- Phillips, R.P., Fahey, T.J., 2006. Tree species and mycorrhizal associations influence the magnitude of rhizosphere effects. *Ecology* 87 (5), 1302–1313. [https://doi.org/10.1890/0012-9658\(2006\)87\[1302:tsamaj\]2.0.co;2](https://doi.org/10.1890/0012-9658(2006)87[1302:tsamaj]2.0.co;2).
- R Core Team, 2019. R: A Language and Environment for Statistical Computing. R Foundation for Statistical Computing, Vienna, Austria. <http://www.R-project.org/>.
- Reddy, I.N.B.L., Kim, B.K., Yoon, I.S., Kim, K.H., Kwon, T.R., 2017. Salt tolerance in rice: focus on mechanisms and approaches. *Rice Sci.* 24 (3), 123–144. <https://doi.org/10.1016/j.rsci.2016.09.004>.
- Saleh, J., Najafi, N., Oustan, S., Aliasgharzad, N., Ghassemi-Golezani, K., 2013. Changes in extractable Si, Fe, and Mn as affected by silicon, salinity, and waterlogging in a sandy loam soil. *Commun. Soil Sci. Plant Anal.* 44 (10), 1588–1598. <https://doi.org/10.1080/00103624.2013.768261>.
- Shao, D., Ruihong, H., Xinzhe, N., Shulan, B., Liang, F., Qin, R., 2008. The study on soil enzyme activity in the *Pinus tabulaeformis* and *Ostryopsis davidiana* rhizosphere in Daqingshan Mountain, Inner Mongolia. *J. Arid Land Resour. Environ.* 22 (6), 190–193 (in Chinese with English abstract).
- Shyla, B., Bhaskar, C.V., Nagendrapa, G., 2012. Iron(III) oxidized nucleophilic coupling of catechol with o-tolidine/p-tolidine followed by 1,10-phenanthroline as new and sensitivity improved spectrophotometric methods for iron present in chemicals, pharmaceutical, edible green leaves, nuts and lake water samples. *Spectrochim. Acta A* 86, 152–158. <https://doi.org/10.1016/j.saa.2011.09.068>.
- Siddiqui, N., Rauf, A., Latif, A., Mahmood, Z., 2017. Spectrophotometric determination of the total phenolic content, spectral and fluorescence study of the herbal Unani drug Gul-e-Zoofa (Nepeta bracteata Benth.). *J. Taibah Univ. Med. Sci.* 12 (4), 360–363. <https://doi.org/10.1016/j.jtumed.2016.11.006>.
- Sowers, T.D., Holden, K.L., Coward, E.K., Sparks, D.L., 2019. Dissolved organic matter sorption and molecular fractionation by naturally occurring bacteriogenic iron (oxyhydr)oxides. *Environ. Sci. Technol.* 53 (8), 4295–4304. <https://doi.org/10.1021/acs.est.9b00540>.
- Tang, Y.S., Wang, L., Jia, W., Fu, H., Le, Y.Q., Chen, X., Sun, Y., 2011. Response of soil microbial community in Jiuduansha wetland to different successional stages and its implications for soil microbial respiration and carbon turnover. *Soil Biol. Biochem.* 43 (3), 638–646. <https://doi.org/10.1016/j.soilbio.2010.11.035>.
- Thompson, A., Chadwick, O.A., Rancourt, D.G., Chorover, J., 2006. Iron-oxide crystallinity increases during soil redox oscillations. *Geochim. Cosmochim. Acta* 70 (7), 1710–1727. <https://doi.org/10.1016/j.gca.2005.12.005>.
- Tomaszewski, E.J., Coward, E.K., Sparks, D.L., 2021. Ionic strength and species drive iron-carbon adsorption dynamics: implications for carbon cycling in future coastal environments. *Environ. Sci. Technol. Lett.* 8, 719–724. <https://doi.org/10.1021/acs.estlett.1c00432>.
- Tong, T., Li, R., Wu, S., Xie, S., 2019. The distribution of sediment bacterial community in mangroves across China was governed by geographic location and eutrophication. *Mar. Pollut. Bull.* 140, 198–203. <https://doi.org/10.1016/j.marpolbul.2019.01.046>.
- Vogelsang, V., Kaiser, K., Wagner, F.E., Jahn, R., Fiedler, S., 2016. Transformation of clay-sized minerals in soils exposed to prolonged regular alternation of redox conditions. *Geoderma* 278, 40–48. <https://doi.org/10.1016/j.geoderma.2016.05.013>.
- Wagai, R., Mayer, L.M., 2007. Sorptive stabilization of organic matter in soils by hydrous iron oxides. *Geochim. Cosmochim. Acta* 71 (1), 25–35. <https://doi.org/10.1016/j.gca.2006.08.047>.
- Wang, J., Zhang, Z., Liang, F., Che, Z., Wen, Y., Zhang, M., Jin, W., Dong, Z., Song, H., 2023. Decreased soil pH weakens the positive rhizosphere effect on denitrification capacity. *Pedosphere*. <https://doi.org/10.1016/j.pedsph.2023.07.011> (in press).
- Weaver, B.L., Tarney, J., 1984. Empirical approach to estimating the composition of the continental crust. *Nature* 310 (5978), 575–577. <https://doi.org/10.1038/310575a0>.
- Weiss, J.V., Emerson, D., Backer, S.M., Megonigal, J.P., 2003. Enumeration of Fe(II)-oxidizing and Fe(III)-reducing bacteria in the root zone of wetland plants: implications for a rhizosphere iron cycle. *Biogeochemistry* 64 (1), 77–96. <https://doi.org/10.1023/A:1024953027726>.
- Wiseman, C.L.S., Püttmann, W., 2006. Interactions between mineral phases in the preservation of soil organic matter. *Geoderma* 134 (1), 109–118. <https://doi.org/10.1016/j.geoderma.2005.09.001>.
- Xie, E., Wei, X., Ding, A., Zheng, L., Wu, X., Anderson, B., 2020. Short-term effects of salt stress on the amino acids of *Phragmites australis* root exudates in constructed wetlands. *Water* 12 (2), 569. <https://doi.org/10.3390/w12020569>.
- Xue, L., Li, X., Yan, Z., Zhang, Q., Ding, W., Huang, X., 2018a. Effects of salinity and inundation on carbon storage of halophytes in the tidal salt marsh of the Yangtze River Estuary, China. *Acta Ecol. Sin.* 38 (9), 2995–3003 (in Chinese with English abstract).
- Xue, L., Li, X., Zhang, Q., Yan, Z., Ding, W., Huang, X., Ge, Z., Tian, B., Yin, Q., 2018b. Elevated salinity and inundation will facilitate the spread of invasive *Spartina alterniflora* in the Yangtze River Estuary, China. *J. Exp. Mar. Biol. Ecol.* 506, 144–154.
- Xue, L., Jiang, J., Li, X., Yan, Z., Zhang, Q., Ge, Z., Tian, B., Craft, C., 2020. Salinity affects topsoil organic carbon concentrations through regulating vegetation structure and productivity. *J. Geophys. Res. Biogeosci.* 125, e2019JG005217. <https://doi.org/10.1029/2019JG005217>.
- Yu, G., 2018. Root Exudates and Microbial Communities Drive Mineral Dissolution and the Formation of Nano-size Minerals in Soils: Implications for Soil Carbon Storage. Springer International Publishing, Root Biology Cham, pp. 143–166.
- Yu, C., Xie, S., Song, Z., Xia, S., Åström, M.E., 2021. Biogeochemical cycling of iron (hydr)-oxides and its impact on organic carbon turnover in coastal wetlands: a global synthesis and perspective. *Earth Sci. Rev.* 218, 103658. <https://doi.org/10.1016/j.earscirev.2021.103658>.
- Yuan, B.C., Li, Z.Z., Liu, H., Gao, M., Zhang, Y.Y., 2007. Microbial biomass and activity in salt affected soils under arid conditions. *Appl. Soil Ecol.* 35 (2), 319–328. <https://doi.org/10.1016/j.apsoil.2006.07.004>.
- Yuan, J., Zhang, N., Huang, Q., Raza, W., Li, R., Vivanco, J.M., Shen, Q., 2015. Organic acids from root exudates of banana help root colonization of PGPR strain *Bacillus amyloliquefaciens* NJN-6. *Sci. Rep.-UK* 5 (1), 13438. <https://doi.org/10.1038/srep13438>.
- Zang, F., Wang, S., Nan, Z., Ma, J., Wang, Y., Chen, Y., Zhang, Q., Li, Y., 2017. Influence of pH on the release and chemical fractionation of heavy metals in sediment from a suburban drainage stream in an arid mine-based oasis. *J. Soils Sediments* 17, 1–13. <https://doi.org/10.1007/s11368-017-1730-4>.
- Zhang, Y., Lin, X., Werner, W., 2003. The effect of soil flooding on the transformation of Fe oxides and the adsorption/desorption behavior of phosphate. *J. Plant Nutr. Soil Sci.* 166 (1), 68–75. <https://doi.org/10.1002/jpln.200390014>.
- Zhang, Q., Yan, Z., Bi, Y., Lei, Y., Gao, X., Li, X., Brix, H., 2023. Iron plaque crystallinity, heavy metal toxicity, and metal translocation in *Kandelia obovata* seedlings as altered by an iron-reducing bacterium under different flooding regimes. *Plant Soil* 487 (1), 267–282. <https://doi.org/10.1007/s11104-023-05924-9>.